



# Atomistic simulation study on the crack growth stability of graphene under uniaxial tension and indentation

Sangryun Lee · Nicola M. Pugno · Seunghwa Ryu 

Received: 14 December 2018 / Accepted: 23 July 2019 / Published online: 31 July 2019  
© Springer Nature B.V. 2019

**Abstract** Combining a series of atomistic simulations with fracture mechanics theory, we systematically investigate the crack growth stability of graphene under tension and indentation, with a pre-existing crack made by two methods: atom removal and (artificial) bonding removal. In the tension, the monotonically increasing energy release rate  $G$  is consistent with the unstable crack growth. In contrast, the non-monotonic  $G$  with a maximum for indentation explains the transition from unstable to stable crack growth when the crack length is comparable to the diameter of the contact zone. We also find that the crack growth stability within a stable crack growth regime can be significantly affected by the crack tip sharpness even down to a single atom scale. A crack made by atom removal starts to grow at a higher

indentation force than the ultimately sharp crack made by bonding removal, which leads to a large force drop at the onset of the crack growth that can cause unstable crack growth under indentation with force control. In addition, we investigate the effect of the offset distance between the indenter and the crack to the indentation fracture force and find that the graphene with a smaller initial crack is more sensitive. The findings reported in this study can be applied to other related 2D materials because crack growth stability is determined primarily by the geometrical factors of the mechanical loading.

**Keywords** Fracture · Graphene · Indentation · Tension · Crack tip blunting

---

S. Lee · S. Ryu (✉)  
Department of Mechanical Engineering and KI for the NanoCentury, Korea Advanced Institute of Science and Technology, Daejeon 34141, Republic of Korea  
e-mail: ryush@kaist.ac.kr

N. M. Pugno  
Laboratory of Bio-Inspired & Graphene Nanomechanics, Department of Civil Environmental and Mechanical Engineering, University of Trento, Via Mesiano 77, 38123 Trento, Italy

N. M. Pugno  
School of Engineering and Materials Science, Queen Mary University of London, Mile End Road, London E1 4NS, UK

## 1 Introduction

Due to its exceptional mechanical [1–3], electronic [4, 5] and thermal properties [6, 7], graphene has been widely used for various applications such as nanocomposites [8, 9], energy storage [10, 11], and conductive electrodes [12, 13]. For the realistic application of graphene, it is important to characterize its intrinsic properties including the mechanical properties such as strength, modulus, and stretchability. Because it is difficult to conduct a uniaxial tension test on the atomically thin layer, the mechanical properties of

graphene have been characterized mostly by nanoindentation tests [2, 14, 15]. The measured mechanical properties of defect-free single crystal graphene are reported to be a Young's modulus of  $\sim 1$  TPa and a strength of  $\sim 120$  GPa, which turns out to be consistent with theoretical predictions [2]. However, there has been some controversy over the strength and modulus of large-area polycrystal graphene synthesized through the CVD process that contains defects such as grain boundaries (GBs) and cracks [16, 17] which promote pre-stress and a stress concentration near the defects [18–21].

The effect of GBs on the material properties of graphene has been investigated by several simulation and experiment studies [22–24]. Five to seven defects along a GB are geometrically necessary to accommodate the misorientation angle between two grains separated by the GB [25, 26]. Several theoretical and computational studies have reported that the dipolar pre-stress from the 5–7 defects is responsible for the reduced tensile strength of polycrystal graphene [19, 21, 22]. In contrast, there exist two different claims about the tensile strength estimated from nanoindentation experiments. Lee et al. [24] has argued that polycrystal graphene is as strong as pristine graphene regardless of the misorientation angle, while Rasool et al. [27] reported that the GB reduces the strength significantly. A previous computational and theoretical study performed by some of us claimed that the fracture force cannot be mapped to the tensile strength [18, 28] because of two reasons: (1) the nanoindentation fracture force for a GB with a small misorientation angle cannot be linked to the onset of crack nucleation while the fracture strength under tension can be linked because of a different crack growth stability for the indentation and tensile loading, and (2) a small offset distance between the indenter tip and the GB (as small as the indenter radius) makes the indentation fracture force be almost identical to that of pristine graphene. The primary origin is suggested to be the fast decaying stress field outside of the contact area which is inversely proportional to the distance  $r$  from the indenter tip. In previous studies, the energy release rate  $G$  has not been directly calculated from atomistic simulations but has been analytically estimated by geometrical argument when the crack length is larger than the diameter of the contact area.

Meanwhile, with the advancement of experimental techniques, uniaxial tension experiments on graphene

have been reported in a few studies. However, due to the difficulty in preparing a dog-bone shape graphene sample (which is necessary to mitigate the stress concentration at the grips), graphene samples with a pre-notched crack using a femto-second laser have been tested for toughness measurements [29]. However, although the crack tip sharpness is known to have an important role down to the atomic scale [30, 31], it is hard to obtain information on the crack tip sharpness from experiments while most atomistic simulations assume a pre-existing crack is made with the removal of a single row of atoms [29, 32–35].

To achieve a deeper understanding, this study investigates the crack growth stability under different loading conditions and its sensitivity to the crack tip sharpness with a pre-existing crack made by two methods, atom removal and (artificial) bonding removal. We directly compute the energy release rates of graphene under two loading conditions which explain the unstable crack growth under tension as well as the transition from an unstable to a stable crack growth regime under indentation when the crack size becomes comparable to the contact zone. Interestingly, the crack growth stability within the stable crack growth regime can be significantly affected by the crack tip sharpness down to a single atom scale. A crack made by atom removal starts to grow at a higher indentation force than the ultimately sharp crack made by bonding removal. This results in a large force drop at the onset of crack growth, which can cause an unstable crack growth under indentation with force control. In addition, we investigate the sensitivity of the indentation results to the offset distance between the indenter and the crack, which is present in realistic experiments, showing that the indentation force for graphene with a smaller initial crack is more sensitive to the offset distance. The findings of this study can be applied to the mechanical testing of other related 2D materials.

## 2 Simulation method

We use the large-scale atomic/molecular massively parallel simulator (LAMMPS) for the molecular dynamics (MD) simulations [36] of a graphene sheet about  $55 \text{ nm} \times 55 \text{ nm}$ . For the indentation modeling, we use the NVT ensemble for the interior circular part with a diameter  $D$  of 50 nm at a temperature of 1 K.

Because internal force in radial direction by the indenting loading is axisymmetric, we fix the exterior part to mimic experimental condition where the graphene is suspended over open hole in substrate. (see Fig. 1). Although we chose 1 K instead of 300 K for the ease of computing the energy release rate and visualizing the stress distribution, the outcome at 300 K is expected to be identical but with a slightly reduced fracture force. The AIREBO potential is used to describe the interaction between carbon atoms [37]. The potential has been widely used in a variety of modeling studies concerning the mechanical testing of carbon material such as polycrystalline diamond [38], graphene [18, 20, 28, 32, 34, 39] or carbon nanotube [40, 41]. It consists of three terms: REBO, LJ, and torsion where LJ is used for long-range atomic interaction and torsional term describes torsional bond interactions. In all of our simulation, we use the sigma scale factor of 3.0 for LJ term in LAMMPS and the cutoff radius of  $r_{cc}$  as 2.0 Å to avoid any non-physical hardening behavior at the low temperature [38, 42]. We consider a frictionless rigid spherical indenter by using an artificial spherical potential field which exerts a repulsive force to the atoms inside the spherical indenter. The force on the graphene atoms is given by  $= -k(r - R)^2$ , where  $k$ ,  $R$  and  $r$  are the spring constant, indenter radius and distance of the atom

from the indenter center, respectively. We use  $k = 10 \text{ eV}/\text{Å}^3$  and  $R = 5 \text{ nm}$  for all calculations. We use a sufficiently large graphene sheet ( $D/R = 10$ ) because the rupture force does not depend on the sample size if the sheet diameter is twice larger than the indenter radius [27, 39]. We create a crack at the center of the graphene sheet using two different methods and consider two different crack orientations, the armchair and zigzag. As shown in Fig. 1, we remove a single atom layer to construct the atom-removal crack which is a realistic pre-existing crack in experiments, while we artificially turn off the interaction between the blue and yellow region by assigning atom indices to construct the bonding removal crack. The crack made by bonding removal can be considered as the ideal sharp crack (see Fig. 1) which appears during dynamic crack growth.

We first obtain the graphene configuration by minimizing the total potential energy using the conjugate gradient method. For the thermal equilibration, we first conduct the NPT ensemble for 5 ps with a timestep of 1 fs to relax the initial stress in the  $xy$  direction and run the NVT ensemble for 5 ps after fixing the outer atoms. The indentation simulation is conducted under the NVT ensemble, and the indenter tip velocity is  $0.02 \text{ Å}/\text{ps}$  in the out of plane ( $z$ ) direction (see the Fig. 1). The indenter tip moves

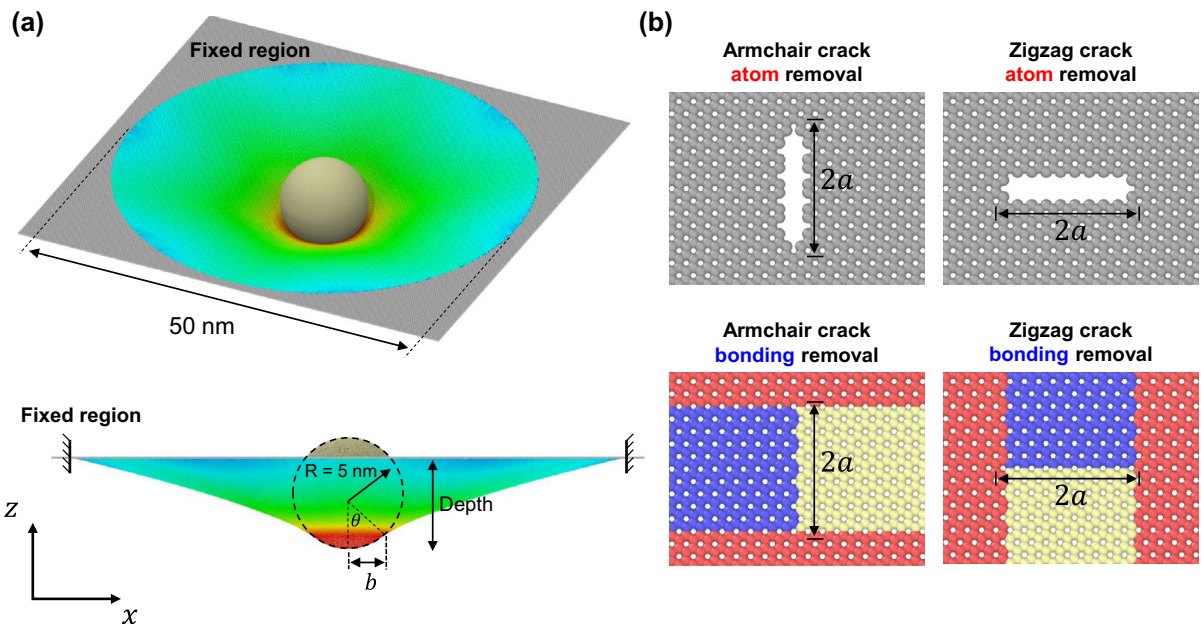


**Fig. 1** a Schematic of the graphene indentation testing. b Four different crack geometries

downwards every 5 ps with a displacement increment of 0.1 Å. The indenting force is measured for the circular clamped graphene sheet and averaged over 2.5 ps at every increment to average out the thermal fluctuation.

The uniaxial tensile test simulation is also performed under 1 K. It is initially equilibrated by the NPT ensemble for 5 ps after minimization; then, the tensile testing is conducted using the NPT ensemble to relax the stress in the lateral direction due to the Poisson effect. The strain rate is  $10^8/s$  with the strain increment of 0.001, so the applied strain increases every 10 ps. At each strain, we calculate the applied stress by averaging the virial stress over last 5 ps out 10 ps equilibration period. We set the thickness of the graphene as 0.33 nm [43] when considering the cross-section area for the stress calculation. The virial theorem and the atomic volume of carbon  $8.8 \text{ \AA}^3$  is used to calculate the atomic stress [18, 22]. All of the simulation results are visualized by OVITO [44].

### 3 Simulation results

We first conduct the indentation testing simulation for pristine graphene as a reference, and the results are shown in Fig. 2. The stress is highly concentrated within the contact area, while the stress beyond the contact area is inversely proportional to the distance  $r$  from the center due to the force equilibrium condition along the indentation direction:

$$F = 2\pi r t \sigma_{rr} \sin \theta, \quad \sigma_{rr} = \frac{F}{2\pi r t \sin \theta} \quad (1)$$

where  $\sigma_{rr}$  is the stress in the radial direction;  $t$  is the thickness of graphene;  $F$  is the indentation force, and  $\theta$  is the angle between the graphene sheet and the plane perpendicular to the indentation force. The pristine graphene shows catastrophic failure with a large indenter force drop after crack nucleation shown in Fig. 2. After crack nucleation, large cracks are formed in multiple directions simultaneously because the highly accumulated strain energy released at the onset of crack nucleation is large enough to create such a large crack edge.

The indentation testing results for the pre-cracked graphene with different crack lengths are shown in Fig. 3. The strength of the pre-cracked graphene is

lower than that of the pristine, regardless of the crack types. For a short crack ( $\sim 1.5$  nm), the initial crack grows instantaneously creating a large crack edge area which implies unstable crack growth; thus, the force drops abruptly during which the crack size becomes larger than the contact zone. Then, it sustains a short period of stable crack growth until the crack size increases so large that it cannot support the indenter tip. This is different from the fracture of the pristine graphene for which the accumulated strain energy before the crack nucleation is so high that the crack grows explosively to a scale much beyond the indenter radius during the first force drop. The results are qualitatively similar between the cracks made by the two methods and also between the armchair and zigzag graphene, except that the fracture force is slightly lower for the bonding removal crack than for the atom removal crack due to the sharper crack tip.

For a larger initial crack length over 5.8 nm, we observe qualitatively different outcomes for cracks made by the two different methods. The indentation force for the bonding removal crack first makes a cusp when the crack growth initiates but with continuous increases and a lower rate without an overshoot because graphene can sustain the indentation load until the crack size becomes significantly higher than the contact zone (as illustrated by Fig. 3a, b). The indentation force at the initiation of crack growth and its rising rate during the stable growth regime are higher for the armchair graphene than for the zigzag graphene because more atomic bonds are required to be broken per unit length for the crack growth (see Fig. 1b). In comparison, the indentation force for the atom removal case shows a notable drop in force at the initiation of crack growth with a sudden increase of the crack length, and eventually follows the identical force–displacement curve with the bonding removal case because the growing crack is identical with the ideal crack tip sharpness. This indicates that even the single atom scale blunted crack induces a noticeable and non-negligible effect on the fracture. The fracture force overshoot has an even more interesting implication when we consider the indentation with force control, or realistic displacement-control indentation experiments where the response time of the feed-back loop of the device is slower than the timescale of the crack growth inside the graphene. For the zigzag case, because the overshoot indentation force at the crack growth initiation is the maximum in the entire force–

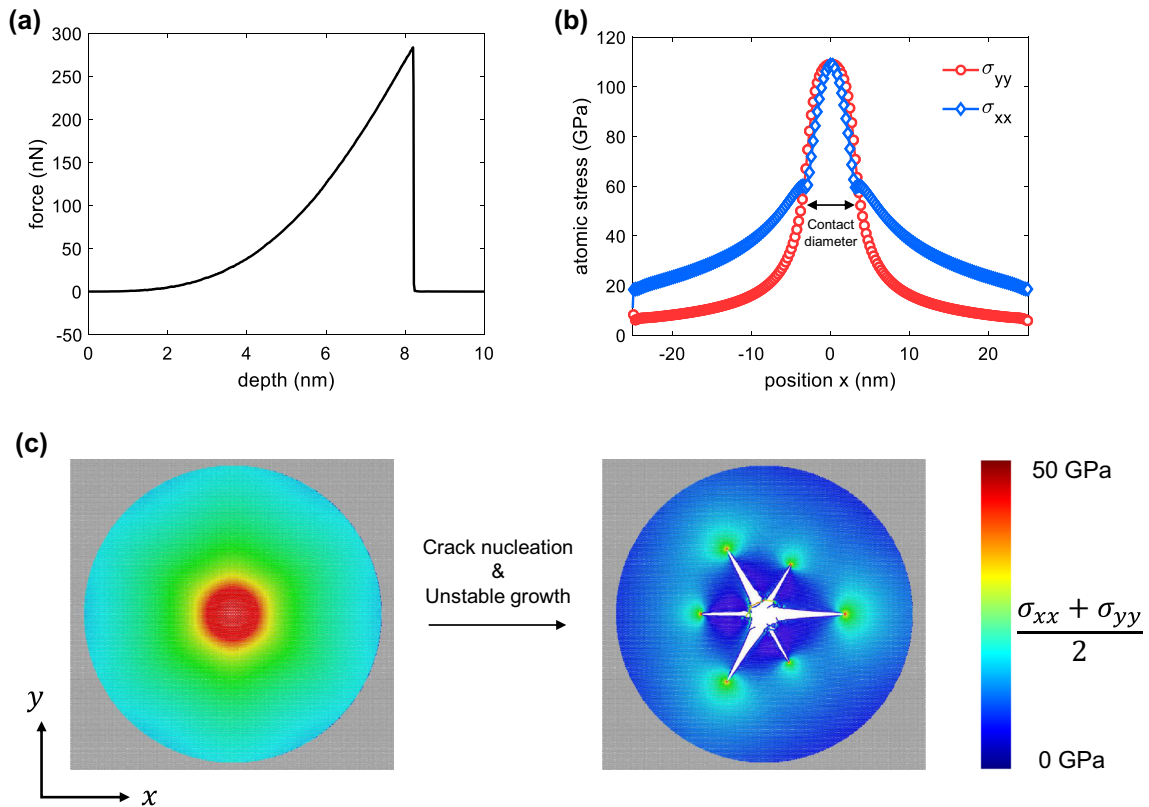


**Fig. 2** **a** Force–depth curve predicted from the pristine graphene indentation testing. **b** Atomic stress distribution along the center line. **c** Stress distribution of the graphene before and after crack nucleation

displacement curves, only the unstable fracture mode can be observed for the graphene containing the pre-existing crack. With a larger initial crack (~ 7 nm), interestingly, the indentation force at the onset of crack growth becomes higher compared to the 5.8 nm case because the crack tip is located further from the indenter center, reducing the stress level at the crack tip at the same indentation depth. Otherwise, the crack growth stability results are qualitatively similar to the ~ 5.8 nm initial crack case.

In the tensile test simulations, the pre-cracked graphene shows catastrophic failure regardless of the initial crack length because the stress field within the entire domain (except the vicinity of the crack) is uniform (see Fig. 3). As shown in Fig. 3, the pre-cracked graphene containing a longer initial crack has a lower strength than that of the short crack graphene, which matches well with the fracture mechanics theory prediction. The difference between the atom removal crack and the bonding removal crack is not significant except for a small difference in the fracture

strength. Because the bonding removal crack is sharper than the atom removal crack, a lower strength is predicted due to a higher stress concentration at the crack tip which is explained by the Inglis solution given as  $\sigma_{max} = \sigma \left( 1 + 2\sqrt{\frac{a}{\rho}} \right)$ , where  $a$  is half of the initial crack length;  $\sigma$  is the applied stress and  $\rho$  is the curvature radius of the crack tip, respectively [45]. “Appendix 1” presents all the force–depth curves from the indentation testing and stress curves from the uniaxial tensile testing considered in the present study.

In Fig. 4, we plot the predicted strength from the indentation and uniaxial testing simulation. For indentation, following the existing experimental and simulation studies [2, 18, 24], we map the indentation force into a strength based on the indenting force–strength relationship of the pristine graphene (obtainable from Fig. 2a, b). Such a strength estimation from the indentation is compared with the fracture strength from the direct uniaxial tensile testing which shows a monotonically decreasing behavior, as expected from

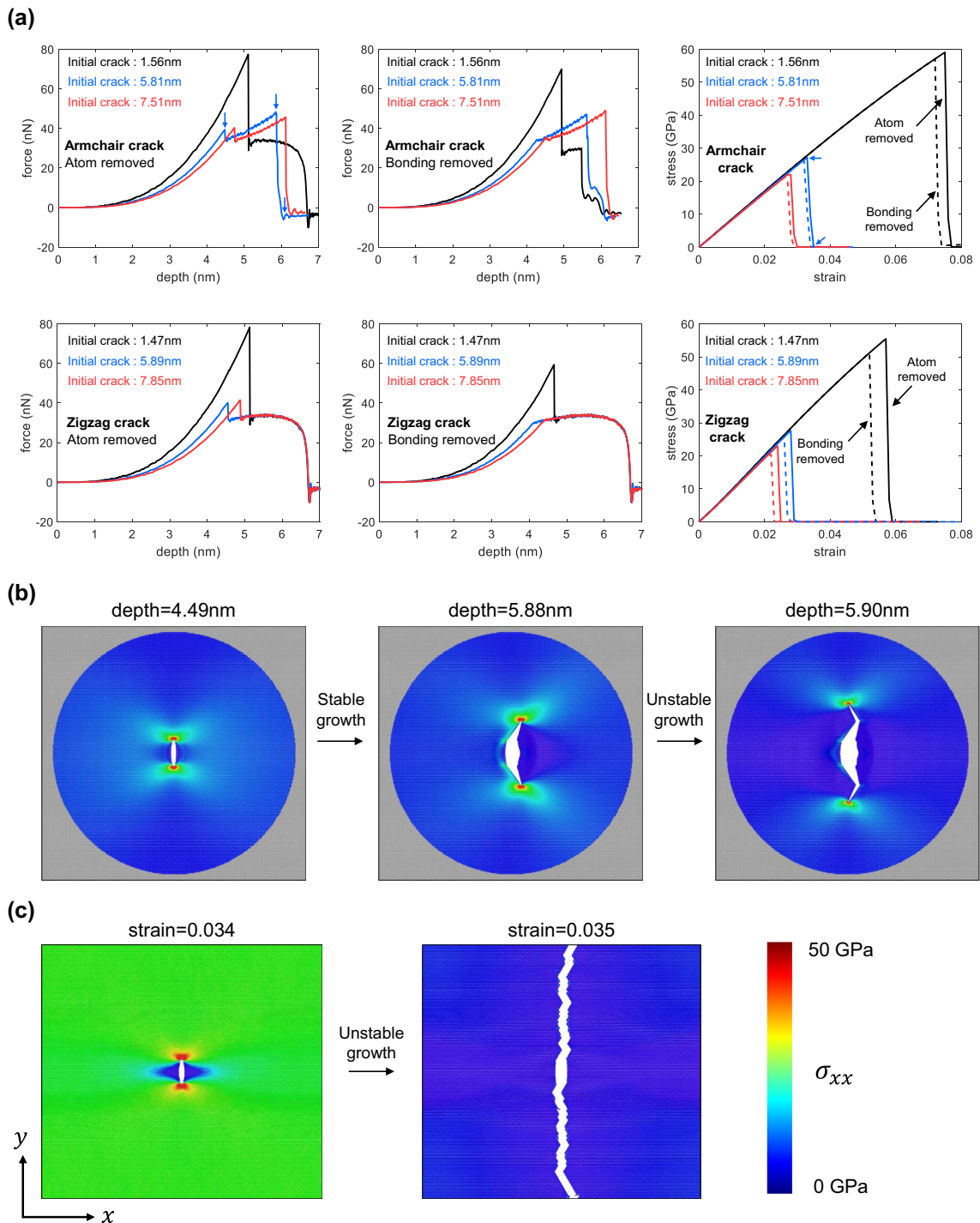


**Fig. 3** a Force–depth curve and stress–strain curve for the pre-cracked graphene. The arrows indicate the snapshot points for **b** and **c** at the indentation and tensile testing, respectively. Atomic

stress  $\sigma_{xx}$  for  $2a = 5.89\text{nm}$  for **b** nanoindentation testing and **c** uniaxial tensile testing

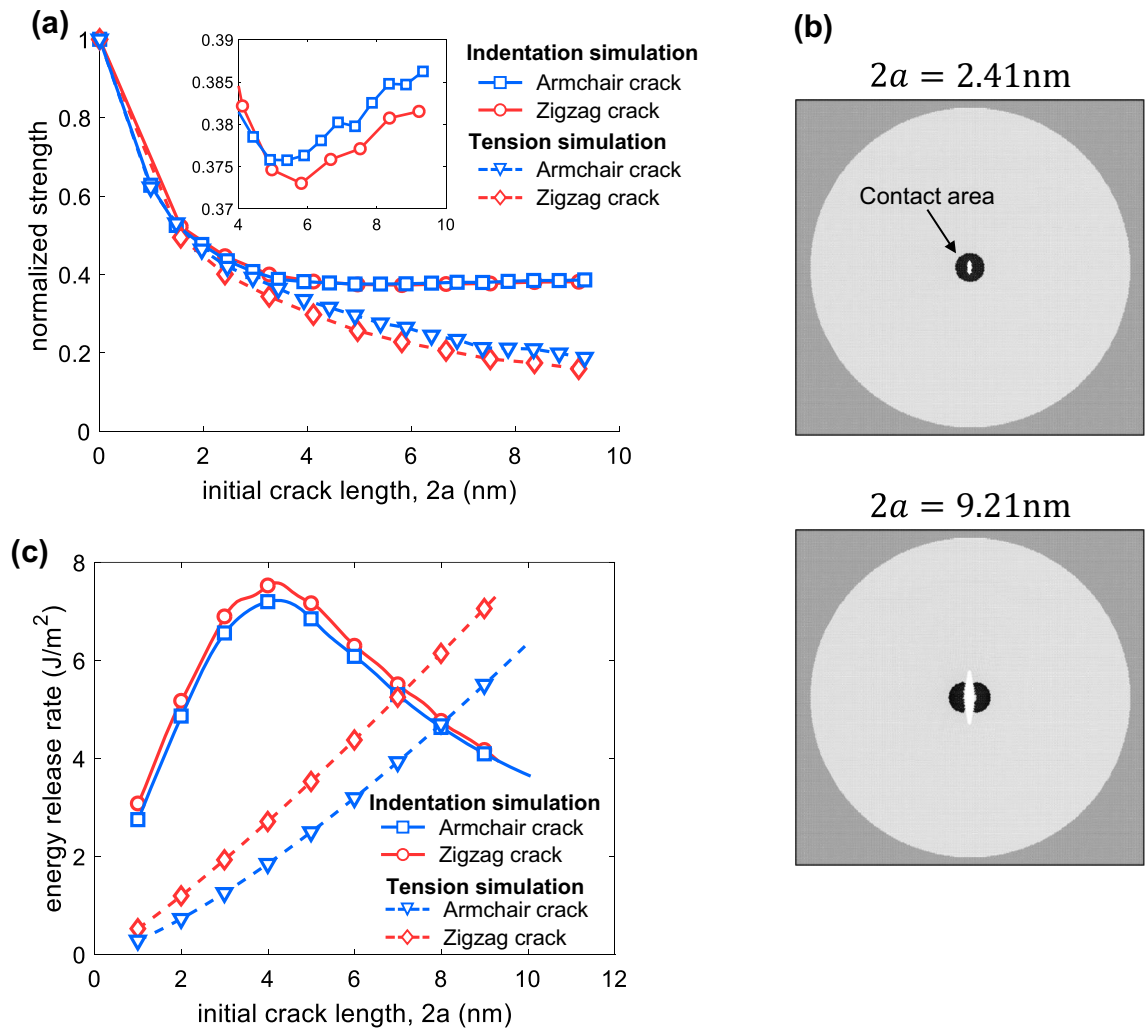


**Fig. 4** **a** Strength predicted from the indentation and tension testing normalized by the pristine strength. **b** The contact area between the graphene and indenter tip just before crack growth initiation. **c** The energy release rate at a constant depth (3.85 nm) and strain (0.018)

the fracture mechanics theory [45]. We find that the estimated normalized strength (ratio to the pristine strength) from the indentation follows that from the uniaxial tension when the crack size is small, and thus, an unstable fracture is observed. However, for the larger initial crack length case where the onset of crack growth occurs when the contact zone is comparable or smaller than the crack size, the estimated strength increases with the initial crack length because the ultimate fracture force increases with the initial crack length in the regime. Hence, the strength estimated from the indentation in the stable crack growth regime shows a different trend compared to the fracture strength from the uniaxial tension.

### 3.1 Elastic fracture mechanics theory

We then make a detailed explanation on the crack growth stability based on the energy release rate ( $G$ ). Because the crack growth stability is similar between the two crack creation methods, we use the configurations with the atom removal crack to obtain  $G$ . Here, we consider  $G$  rather than the stress intensity factor ( $K_{I,II,III}$ ) which is frequently used in other studies [29, 32, 33] because the graphene shows a significantly nonlinear stress–strain behavior with a large stretchability and a maximum strain of about  $\sim 20\%$  (see “Appendix 2”). For displacement control, the energy release rate can be obtained as follows:

$$G = -\frac{\partial F}{\partial a} \quad (2)$$

where  $F$  is the Helmholtz free energy. Because the temperature in our simulation is about 1 K, the entropic effect is negligible compared to the potential energy. Hence, at a low temperature, we calculate the energy release rate as follows:

$$G = -\frac{\partial F}{\partial a} = -\frac{\partial(\Pi - TS)}{\partial a} \approx -\frac{\partial \Pi}{\partial a} \quad (3)$$

where  $\Pi$  is the total potential energy which is the strain energy obtained from the simulation. We can compute  $G$  from the derivative of the smoothed  $a$  versus  $\Pi$  curves from direct atomistic calculation by spline fitting. From the elastic fracture mechanics with the

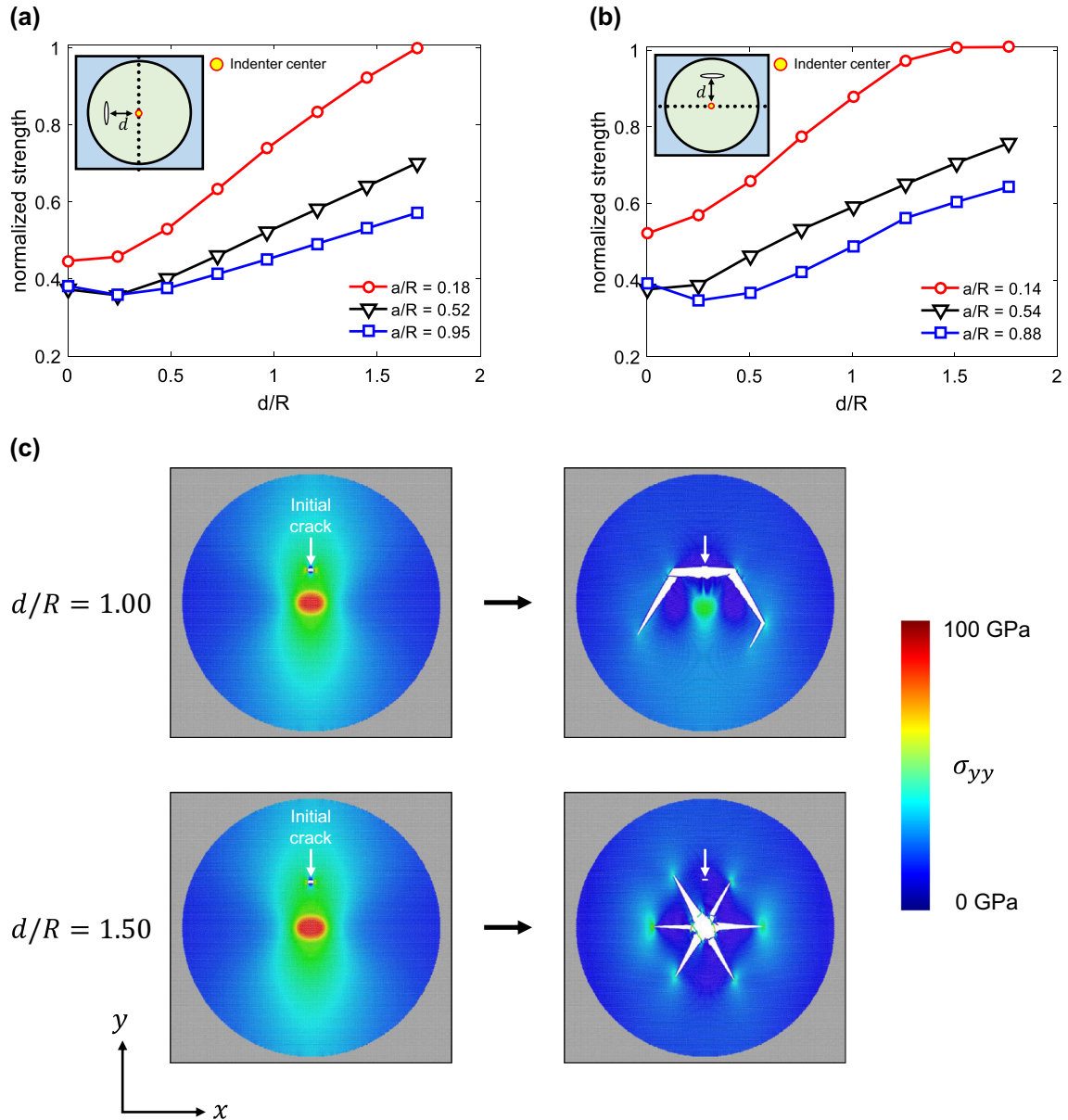


**Fig. 5** Strength prediction for the indentation testing when the initial crack (**a** armchair, **b** zigzag) is shifted from the indenter tip. **c** Atomic stress  $\sigma_{yy}$  distribution for  $a/R = 0.18$ . The arrows indicate the initial crack position

energy release rate, the crack growth initiation and stability can be predicted as follows:

$$\begin{aligned}
 G = G_c &: \text{ Crack growth initiation} \\
 \left. \frac{\partial G}{\partial a} \right|_{G=G_c} < 0 &: \text{ Stable crack growth} \\
 \left. \frac{\partial G}{\partial a} \right|_{G=G_c} > 0 &: \text{ Unstable crack growth}
 \end{aligned}
 \tag{4}$$

where  $G_c$  is the material-dependent critical energy release rate.

As shown in Fig. 4, the energy release rate from the tensile testing is a monotonically increasing function, which implies the crack grows unstably regardless of the initial crack length. The graphene with the zigzag oriented initial crack has a higher energy release rate under a fixed displacement because the surface (edge) energy in the zigzag direction is lower than that of the armchair direction [33]. Due to its lower surface (edge) energy, the crack is likely to grow in the zigzag orientation crack; thus, crack kinking in the initial armchair orientation is captured (see Fig. 3).

The energy release rate from the indentation testing results is an increasing function when the initial crack is shorter than the contact diameter, which is consistent with the unstable crack growth observed in the atomistic simulations. With a longer initial crack, the sign of  $\frac{\partial G}{\partial a}$  is changed from positive to negative, implying that crack growth stability is changed from unstable to stable growth. The transition occurs when the initial crack length is comparable to the size of the contact zone (see Fig. 4).

### 3.2 Initial crack: indenter misalignment

All previous results are obtained when the indenter tip is located right at the center of the initial crack. However, in experiments, it is hard to locate the indenter tip on the top of the defect exactly. Hence, we study the effect of the offset distance between the indenter tip and crack on the fracture behavior. We conduct MD simulations for the pre-cracked graphene for which the initial crack is located slightly away from the center of the graphene and compute the strength (mapped from the indentation fracture force) with respect to the misalignment distance ( $d$ ). As shown in Fig. 5, the estimated strength is recovered to

the strength of the pristine graphene as the offset distance increases.

The strength of graphene with a short crack is almost recovered to the strength of pristine graphene when the offset distance is larger than  $1.5R$  whereas the strength of graphene with a larger crack in the graphene is still less than that of the pristine graphene at the same offset distance. For a short offset distance of  $d/R = 1$ , the crack growth initiates at the crack tip, and it propagates following the zigzag direction which has a low surface (edge) energy (see Fig. 5). When the crack is sufficiently far away from the indenter tip ( $d/R = 1.5$ ), the stress field at the tip is higher than the stress at the crack tip. Accordingly, the crack nucleates at the center of the contact area, and it shows catastrophic failure creating a large crack surface instantaneously, which is very similar with the fracture pattern of the pristine graphene (see Figs. 2, 5).

## 4 Conclusion

In the present study, we systematically investigate the crack growth stability of graphene under tension and indentation by combining atomistic simulations and fracture mechanics theory. The crack growth stability observed in the two loading conditions are explained by the energy release rates directly obtained from atomistic calculations, and the effect of the crack tip sharpness is also discussed by comparing the results on the initial cracks made by atom removal and bonding removal methods. We found that the crack tip sharpness plays an important role below single atom scale: such effect can be quantified by quantum fracture mechanics framework by appropriately accounting for the nonlinear response of graphene [30, 31]. Moreover, we examine the sensitivity of the indentation fracture force to the offset distance from the initial crack. Our findings imply that the stable crack growth mode for larger crack as well as the sensitivity to the offset distance for indentation may lead to an incorrect strength estimation and also that even the blunting of the single atomic scale crack tip can induce a notable difference in the fracture behavior. Our reports can serve as a guideline for the design and interpretation of indentation experiments and simulations on graphene as well as other related 2D materials.

**Acknowledgements** This work is supported by the Basic Science Program through the National Research Foundation of Korea(NRF) funded by the Ministry of Science and ICT (NRF-2019R1A2C4070690). NMP is supported by the European Commission under the Graphene Flagship Core 2 Grant No. 785219 (WP14 “Composites”) and FET Proactive “Neurofibres” Grant No. 732344 as well as by the Italian Ministry of Education, University and Research (MIUR) under the “Departments of Excellence” Grant L.232/2016 and ARS01-01384-PROSCAN Grant.

### Appendix 1: force–depth and stress–strain curve of all pre-cracked graphene

We draw the results for all the indentation testing and uniaxial testing for all pre-cracked graphene (see Fig. 6). For the armchair (zigzag) crack, the shortest and longest initial crack lengths are 1.56 nm (0.984 nm) and 12.6 nm (9.33 nm), respectively, and the interval between the crack lengths is 0.85 nm(0.49 nm).

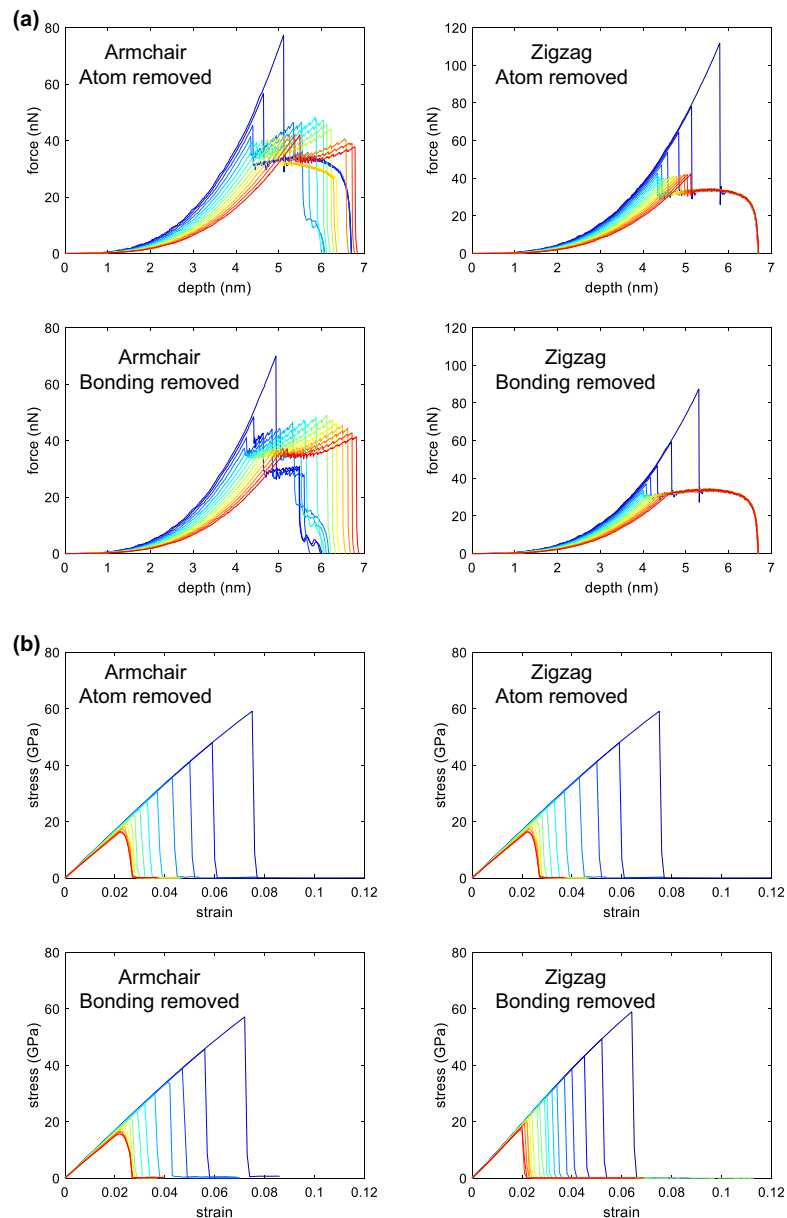


**Fig. 6** a force–depth and b stress–strain curve for all pre-cracked graphene

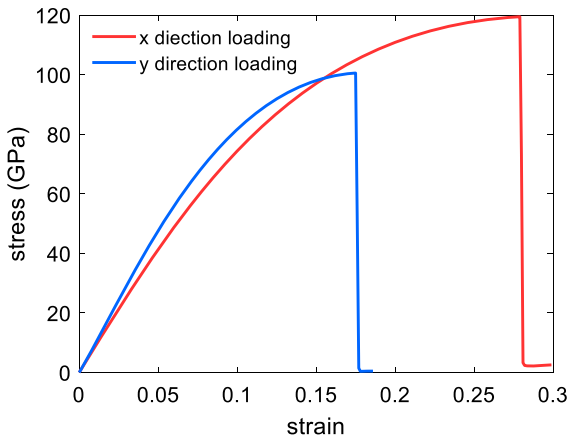


**Fig. 7** stress-strain curve of the pristine graphene under two different loading directions, *x* (zigzag) and *y* (armchair)

## Appendix 2: nonlinear stress–strain curve of the pristine graphene

We plot the stress–strain curves of the pristine graphene for two different loading directions to show that the graphene is an anisotropic material with a nonlinear response. As shown in Fig. 7, the graphene has a high stretchability with a maximum elongation limit of 20%. Accordingly, the energy release rate is more suitable than the stress intensity factor (which is only valid for linear elastic materials) for accurately predicting the crack growth stability.

## References

- Bunch JS, van der Zande AM, Verbridge SS, Frank IW, Tanenbaum DM, Parpia JM, Craighead HG, McEuen PL (2007) Electromechanical resonators from graphene sheets. *Science* 315(5811):490–493
- Lee C, Wei XD, Kysar JW, Hone J (2008) Measurement of the elastic properties and intrinsic strength of monolayer graphene. *Science* 321(5887):385–388
- Koenig SP, Boddeti NG, Dunn ML, Bunch JS (2011) Ultrastrong adhesion of graphene membranes. *Nat Nanotechnol* 6(9):543–546
- Novoselov KS, Geim AK, Morozov SV, Jiang D, Zhang Y, Dubonos SV, Grigorieva IV, Firsov AA (2004) Electric field effect in atomically thin carbon films. *Science* 306(5696):666–669
- Zhang YB, Tan YW, Stormer HL, Kim P (2005) Experimental observation of the quantum Hall effect and Berry's phase in graphene. *Nature* 438(7065):201–204
- Balandin AA, Ghosh S, Bao WZ, Calizo I, Teweldebrhan D, Miao F, Lau CN (2008) Superior thermal conductivity of single-layer graphene. *Nano Lett* 8(3):902–907
- Balandin AA (2011) Thermal properties of graphene and nanostructured carbon materials. *Nat Mater* 10(8):569–581
- Zaman I, Phan TT, Kuan HC, Meng QS, La LTB, Luong L, Youssif O, Ma J (2011) Epoxy/graphene platelets nanocomposites with two levels of interface strength. *Polymer* 52(7):1603–1611
- Rafiee MA, Rafiee J, Srivastava I, Wang Z, Song HH, Yu ZZ, Koratkar N (2010) Fracture and Fatigue in Graphene Nanocomposites. *Small* 6(2):179–183
- Yang XW, Cheng C, Wang YF, Qiu L, Li D (2013) Liquid-mediated dense integration of graphene materials for compact capacitive energy storage. *Science* 341(6145):534–537
- Raccichini R, Varzi A, Passerini S, Scrosati B (2015) The role of graphene for electrochemical energy storage. *Nat Mater* 14(3):271–279
- Li XS, Zhu YW, Cai WW, Borysiak M, Han BY, Chen D, Piner RD, Colombo L, Ruoff RS (2009) Transfer of large-area graphene films for high-performance transparent conductive electrodes. *Nano Lett* 9(12):4359–4363
- Gomez H, Ram MK, Alvi F, Villalba P, Stefanakos E, Kumar A (2011) Graphene-conducting polymer nanocomposite as novel electrode for supercapacitors. *J Power Sources* 196(8):4102–4108
- Berciaud S, Ryu S, Brus LE, Heinz TF (2009) Probing the intrinsic properties of exfoliated graphene: Raman spectroscopy of free-standing monolayers. *Nano Lett* 9(1):346–352
- Garcia-Sanchez D, van der Zande AM, Paulo AS, Lassagne B, McEuen PL, Bachtold A (2008) Imaging mechanical vibrations in suspended graphene sheets. *Nano Lett* 8(5):1399–1403
- Cao HL, Yu QK, Jauregui LA, Tian J, Wu W, Liu Z, Jalilian R, Benjamin DK, Jiang Z, Bao J, Pei SS, Chen YP (2010) Electronic transport in chemical vapor deposited graphene synthesized on Cu: quantum Hall effect and weak localization. *Appl Phys Lett* 96(25):122106
- Reina A, Jia XT, Ho J, Nezich D, Son HB, Bulovic V, Dresselhaus MS, Kong J (2009) Large area, few-layer graphene films on arbitrary substrates by chemical vapor deposition. *Nano Lett* 9(1):30–35
- Han J, Pugno NM, Ryu S (2015) Nanoindentation cannot accurately predict the tensile strength of graphene or other 2D materials. *Nanoscale* 7(38):15672–15679
- Grantab R, Shenoy VB, Ruoff RS (2010) Anomalous strength characteristics of tilt grain boundaries in graphene. *Science* 330(6006):946–948
- Han J, Ryu S, Sohn D, Im S (2014) Mechanical strength characteristics of asymmetric tilt grain boundaries in graphene. *Carbon* 68:250–257
- Wei YJ, Wu JT, Yin HQ, Shi XH, Yang RG, Dresselhaus M (2012) The nature of strength enhancement and weakening by pentagon-heptagon defects in graphene. *Nat Mater* 11(9):759–763
- Liu TH, Pao CW, Chang CC (2012) Effects of dislocation densities and distributions on graphene grain boundary failure strengths from atomistic simulations. *Carbon* 50(10):3465–3472

23. Yi LJ, Yin ZN, Zhang YY, Chang TC (2013) A theoretical evaluation of the temperature and strain-rate dependent fracture strength of tilt grain boundaries in graphene. *Carbon* 51:373–380
24. Lee G-H, Cooper RC, An SJ, Lee S, van der Zande A, Petrone N, Hammerberg AG, Lee C, Crawford B, Oliver W, Kysar JW, Hone J (2013) High-strength chemical-vapor-deposited graphene and grain boundaries. *Science* 340(6136):1073
25. Meyer JC, Geim AK, Katsnelson MI, Novoselov KS, Booth TJ, Roth S (2007) The structure of suspended graphene sheets. *Nature* 446(7131):60–63
26. Kim K, Lee Z, Regan W, Kisielowski C, Crommie MF, Zettl A (2011) Grain boundary mapping in polycrystalline graphene. *ACS Nano* 5(3):2142–2146
27. Rasool HI, Ophus C, Klug WS, Zettl A, Gimzewski JK (2013) Measurement of the intrinsic strength of crystalline and polycrystalline graphene. *Nat Commun* 4:2811
28. Han J, Ryu S, Sohn D (2016) A feasibility study on the fracture strength measurement of polycrystalline graphene using nanoindentation with a cylindrical indenter. *Carbon* 107:310–318
29. Zhang P, Ma LL, Fan FF, Zeng Z, Peng C, Loya PE, Liu Z, Gong YJ, Zhang JN, Zhang XX, Ajayan PM, Zhu T, Lou J (2014) Fracture toughness of graphene. *Nat Commun* 5:3782
30. Pugno N, Carpinteri A, Ippolito M, Mattoni A, Colombo L (2008) Atomistic fracture: QFM vs. MD. *Eng Fract Mech* 75(7):1794–1803. <https://doi.org/10.1016/j.engfracmech.2007.01.028>
31. Pugno NM, Ruoff RS (2004) Quantized fracture mechanics. *Philos Mag* 84(27):2829–2845
32. Han J, Sohn D, Woo W, Kim DK (2017) Molecular dynamics study of fracture toughness and trans-intergranular transition in bi-crystalline graphene. *Comp Mater Sci* 129:323–331
33. Yin HQ, Qi HJ, Fan FF, Zhu T, Wang BL, Wei YJ (2015) Griffith criterion for brittle fracture in graphene. *Nano Lett* 15(3):1918–1924
34. Zhao H, Aluru NR (2010) Temperature and strain-rate dependent fracture strength of graphene. *J Appl Phys* 108(6):064321
35. Meng FC, Chen C, Song J (2017) Lattice trapping and crack decohesion in graphene. *Carbon* 116:33–39
36. Plimpton S (1995) Fast parallel algorithms for short-range molecular-dynamics. *J Comput Phys* 117(1):1–19
37. Stuart SJ, Tutein AB, Harrison JA (2000) A reactive potential for hydrocarbons with intermolecular interactions. *J Chem Phys* 112(14):6472–6486
38. Shenderova OA, Brenner DW, Omeltchenko A, Su X, Yang LH (2000) Atomistic modeling of the fracture of polycrystalline diamond. *Phys Rev B* 61(6):3877–3888
39. Costescu BI, Grater F (2014) Graphene mechanics: II. Atomic stress distribution during indentation until rupture. *Phys Chem Chem Phys* 16(24):12582–12590
40. Umeno Y, Yachi Y, Sato M, Shima H (2019) On the atomistic energetics of carbon nanotube collapse from AIR-EBO potential. *Physica E* 106:319–325
41. Dilrukshi KGS, Dewapriya MAN, Puswewala UGA (2015) Size dependency and potential field influence on deriving mechanical properties of carbon nanotubes using molecular dynamics. *Theor Appl Mech Lett* 5(4):167–172. <https://doi.org/10.1016/j.taml.2015.05.005>
42. Zhang T, Li X, Gao H (2014) Designing graphene structures with controlled distributions of topological defects: a case study of toughness enhancement in graphene ruga. *Extrem Mech Lett* 1:3–8. <https://doi.org/10.1016/j.eml.2014.12.007>
43. Ni ZH, Wang HM, Kasim J, Fan HM, Yu T, Wu YH, Feng YP, Shen ZX (2007) Graphene thickness determination using reflection and contrast spectroscopy. *Nano Lett* 7(9):2758–2763
44. Stukowski A (2010) Visualization and analysis of atomistic simulation data with OVITO—the open visualization tool. *Mod Simul Mater Sc* 18(1):015012
45. Anderson TL (2017) Fracture mechanics: fundamentals and applications. CRC Press, Boca Raton

**Publisher's Note** Springer Nature remains neutral with regard to jurisdictional claims in published maps and institutional affiliations.